





# Magnetically Driven Baryon Winds from Binary Neutron Star Merger Remnants and the Blue Kilonova of 2017 August

Riccardo Ciolfi<sup>1,2</sup>  and Jay Vijay Kalinani<sup>2,3</sup> 

<sup>1</sup> INAF, Osservatorio Astronomico di Padova, Vicolo dell’Osservatorio 5, I-35122 Padova, Italy; [riccardo.ciolfi@inaf.it](mailto:riccardo.ciolfi@inaf.it)

<sup>2</sup> INFN, Sezione di Padova, Via Francesco Marzolo 8, I-35131 Padova, Italy

<sup>3</sup> Università di Padova, Dipartimento di Fisica e Astronomia, Via Francesco Marzolo 8, I-35131 Padova, Italy

Received 2020 July 20; revised 2020 August 19; accepted 2020 August 25; published 2020 September 10

## Abstract

The observation of a radioactively powered kilonova associated with the first binary neutron star (BNS) merger detected in gravitational waves proved that these events are ideal sites for the production of heavy  $r$ -process elements. However, the physical origin of the ejected material responsible for the early (“blue”) and late (“red”) components of this kilonova is still debated. Here, we investigate the possibility that the early/blue kilonova originated from the magnetically driven baryon wind launched after merger by the metastable neutron star remnant. Exploiting a magnetized BNS merger simulation with over 250 ms of post-merger evolution, we can follow for the first time the full mass-ejection process up to its final decline. We find that the baryon wind carries  $\simeq 0.010\text{--}0.028 M_{\odot}$  of unbound material, proving that the high mass estimated for the blue kilonova can be achieved. We also find expansion velocities of up to  $\sim 0.2c$ , consistent with the lower end of the observational estimates, and we discuss possible effects neglected here that could further increase the final ejecta velocity. Overall, our results show that the magnetically driven baryon wind represents a viable channel to explain the blue kilonova.

*Unified Astronomy Thesaurus concepts:* Neutron stars (1108); Compact binary stars (283); Magnetohydrodynamical simulations (1966); Gamma-ray bursts (629); Gravitational wave sources (677)

## 1. Introduction

The first combined gravitational wave (GW) and electromagnetic (EM) observation of a binary neutron star (BNS) merger in 2017 August marked a major milestone in the investigation of these systems (Abbott et al. 2017a, 2017b, 2017c). Among a number of key discoveries, this event provided compelling evidence that BNS mergers can produce a copious amount of heavy  $r$ -process elements up to atomic mass numbers well above  $A = 140$  (e.g., Kasen et al. 2017; Pian et al. 2017), in agreement with decades of theoretical predictions (Lattimer & Schramm 1974; Symbalisty & Schramm 1982). Such confirmation was enabled by the detection and characterization of the ultraviolet (UV)/optical/infrared (IR) signal AT 2017gfo, which was fully consistent with the characteristics of a kilonova, i.e., a thermal transient powered by the radioactive decay of the heavy elements synthesized within the material ejected during and after merger (Li & Paczyński 1998; Metzger et al. 2010).

Despite the overall consistency with a radioactively powered kilonova, however, the interpretation of AT 2017gfo in terms of specific source properties remains challenging, not only due to uncertainties in the involved microphysics, but also because the observed signal may result from a complex combination of contributions from different ejecta components (e.g., Metzger 2019; Siegel 2019). In particular, the analysis of the UV/optical/IR data showed that the simplest kilonova model based on isotropic ejecta with constant opacity and characteristic radial velocity does not provide a satisfactory description, suggesting instead the presence of at least two distinct ejecta components, respectively explaining an early “blue kilonova,” peaking  $\sim 1$  day after merger at UV/blue wavelengths, and a following “red kilonova,” peaking  $\sim 1$  week after merger in the IR band (e.g., Cowperthwaite et al. 2017; Kasen et al. 2017; Pian et al. 2017; Villar et al. 2017). The physical origin and

properties of these two components are still a matter of debate (e.g., Kawaguchi et al. 2018; Metzger et al. 2018; Siegel & Metzger 2018; Nedora et al. 2019), as is the possibility of more than two distinct contributions (e.g., Perego et al. 2017; Villar et al. 2017).

Here, we focus the attention on the origin of the blue kilonova, for which the inferred ejecta properties combine a relatively low opacity of  $\simeq 0.5 \text{ cm}^2 \text{ g}^{-1}$  with a rather high mass of  $\simeq 0.015\text{--}0.025 M_{\odot}$  and a velocity as high as  $\simeq 0.2\text{--}0.3c$  (e.g., Cowperthwaite et al. 2017; Kasen et al. 2017; Pian et al. 2017; Villar et al. 2017). Shock-driven dynamical ejecta can easily reach these velocities, and part of the material could even maintain a low enough opacity, but the mass of the low-opacity portion may be insufficient to fully explain the inferred value (e.g., Bauswein et al. 2013; Hotokezaka et al. 2013; Radice et al. 2016, but see also Nedora et al. 2019). On the other hand, post-merger baryon winds launched by the accretion disk surrounding a newly formed black hole (BH) can accommodate very high masses and a wide range of opacities, but their typical velocity is limited to  $\sim 0.1c$  (e.g., Siegel & Metzger 2018). A third option, which is somewhat intermediate, is the baryon wind launched by the (meta)stable massive neutron star (MNS) remnant prior to its eventual collapse to a BH (if any). As pointed out, e.g., in Metzger et al. (2018), the ongoing neutrino emission from the MNS can significantly raise the electron fraction of the wind material, suppressing the nucleosynthesis of the heaviest elements ( $A > 140$ ) and thus keeping the opacity low (e.g., Perego et al. 2014), and, at the same time, the wind velocity and mass flow rate can be significantly enhanced by the presence of a strong magnetic field. While the magnetically enhanced MNS wind appears as a promising alternative, however, the possibility of reaching high enough ejecta mass and velocity remains to be demonstrated in actual BNS merger simulations.

In this Letter, we address the question of the viability of the magnetically driven baryon wind from the MNS remnant as an explanation for the blue kilonova in AT 2017gfo. We do so by analyzing the outcome of a general relativistic magnetohydrodynamics simulation of a BNS merger with over 250 ms of MNS remnant evolution.<sup>4</sup> To date, this is the only simulation showing the emergence of a helical magnetic field structure and a collimated outflow along the MNS rotation axis as a natural consequence of the merger and post-merger dynamics<sup>5</sup> (where a similar outcome was previously obtained for accreting BH remnants; Ruiz et al. 2016). Our study does not include neutrino radiation or a proper assessment of the ejecta composition, and as such it is not aimed at producing kilonova lightcurves to be directly compared with the observations. Our aim is to show, through an example model, that a magnetically enhanced MNS wind can actually lead to an ejecta component as massive and fast as Required by the observed blue kilonova.

The very long post-merger evolution allows us, for the first time, to follow the specific mass-ejection process associated with the magnetically driven wind until the mass flow rate has substantially declined, after which a further extrapolation in time becomes reliable. In turn, we can reconstruct the full time profile of the mass flow rate at a given distance, as well as the maximum ejecta mass attainable for a sufficiently long-lived MNS. For the case at hand, we obtain a mass of the unbound wind material in the range  $\simeq 0.010\text{--}0.028 M_{\odot}$ , where most of the mass ejection (90%) takes place between about 50 and 190 ms after merger. This demonstrates that matching the mass requirement for the blue kilonova in AT 2017gfo is possible. Moreover, we find ejecta radial velocities distributed in the range  $\simeq 0.1\text{--}0.2c$  (with a maximum of  $0.22c$ ), showing how the additional contribution of magnetic pressure can significantly enhance the velocity of the MNS wind (otherwise limited to  $\lesssim 0.1c$ ). Compared to the blue kilonova estimates, these velocities are consistent with the lower end of the inferred range. We also discuss various effects not included here that may further increase the ejecta velocities.

Overall, our findings support the MNS wind as a viable source for the blue kilonova, thus encouraging further investigation in this direction.

## 2. BNS Model and Numerical Setup

The BNS merger under consideration has the same chirp mass as inferred for the GW170817 event (Abbott et al. 2019) and a mass ratio of  $q \simeq 0.9$  (well inside the estimated range). Neutron star (NS) matter is described via the piecewise-polytropic approximation of the APR4 equation of state (EOS; Akmal et al. 1998; see also Endrizzi et al. 2016), which leads to a MNS remnant that survives without collapsing to a BH for the full extent of the simulation.

Initial dipolar magnetic fields are imposed within the two NSs with maximum field strength of  $5 \times 10^{15}$  G and the total initial magnetic energy is  $E_{\text{mag}} \simeq 4 \times 10^{47}$  erg. Such a high initial field strength allows us to reproduce the expected post-merger magnetization level ( $E_{\text{mag}} \sim 10^{51}$  erg) despite the fact that the early magnetic field amplification, in particular via the

Kelvin–Helmholtz instability (e.g., Kiuchi et al. 2015), is not fully resolved. As discussed in more detail in Ciolfi et al. (2019) and Ciolfi (2020a), the magnetohydrodynamic evolution is rather well resolved starting from  $\sim 30$  to 40 ms after merger, giving us confidence that our qualitative description of the relevant physical effects taking place at later times (including magnetically driven mass ejection) is not affected by the lack of resolution. Nonetheless, we caution that a future investigation based on a much higher resolution (beyond our present capabilities) will be necessary for an accurate quantitative assessment of the ejecta properties and the associated numerical error.

The employed numerical codes and setup are those specified in Ciolfi (2020a). In particular, we recall that the artificial floor density is set to  $\rho_{\text{atm}} \simeq 6.3 \times 10^4 \text{ g cm}^{-3}$ . This corresponds to a mass of  $\simeq 2 \times 10^{-3} M_{\odot}$  within a sphere of radius 2360 km, which is the largest distance at which we monitor matter outflows. The ejecta component of interest carries a mass that is one order of magnitude higher, ensuring that the effects of the floor density could at most represent a small correction. Nonetheless, the possibility that this could slightly slow down the ejecta expansion at the largest distances should be taken into account (see the discussion in Section 3).

## 3. Analysis of the MNS Wind Component of the Ejecta

The merger product is a magnetized MNS remnant characterized by strong differential rotation (Ciolfi 2020a). The Kelvin–Helmholtz instability in the first few ms after merger (e.g., Kiuchi et al. 2015, 2018) and the magnetorotational instability later on (e.g., Balbus & Hawley 1991; Siegel et al. 2013) amplify the magnetic field by orders of magnitude up to a physical saturation achieved around 50 ms after merger, corresponding to  $E_{\text{mag}} \sim 10^{51}$  erg (Ciolfi 2020a). During this phase, the build-up of magnetic pressure drives a baryon-loaded wind that pollutes the environment around the MNS. As the overall magnetic field structure is still quite disordered, the mass outflow is nearly isotropic (e.g., Siegel et al. 2014; Ciolfi et al. 2019).

As the evolution proceeds, the magnetic field gradually acquires a helical structure along the MNS spin axis that enhances the outward acceleration in such direction, resulting in a faster component of outflowing material that starts emerging  $\approx 100$  ms after merger (Ciolfi 2020a).<sup>6</sup> As illustrated in Figure 1, the faster outflow interacts then with the slower and more isotropic surrounding material, eventually leading to a wide-angle ejecta component with a velocity profile that is maximum along the axis and declines at higher polar angles. At the end of the simulation, further mass ejection is significantly reduced, while the material that remained bound starts to slowly fall back toward the MNS.

The time evolution of the mass flow rate across spherical surfaces of different radius is shown in Figure 2, along with the corresponding cumulative mass. In particular, we report the result for 1180 and 2360 km distance and for both the total mass and the unbound mass. To define the unbound mass, we

<sup>4</sup> Some first results from this simulation were presented in Ciolfi (2020a), where the discussion was entirely focused on the prospects of jet formation and the possible connection with short gamma-ray bursts.

<sup>5</sup> This is different from, e.g., Mösta et al. (2020), where a strong, extended dipolar field aligned with the MNS spin is imposed by hand at an arbitrary time early after merger.

<sup>6</sup> The basic mechanism behind this further acceleration along the spin axis is analogous to the one at play when a strong large-scale dipolar field is superimposed by hand on a non-magnetized differentially rotating NS (Shibata et al. 2011; Kiuchi et al. 2012; Siegel et al. 2014; Ruiz et al. 2018; Mösta et al. 2020). However, while the emergence of a collimated outflow is ubiquitous in the latter setup, the same outcome is not always guaranteed for a more realistic magnetic field evolution through the BNS merger (see the discussion in Ciolfi 2020a, 2020b).

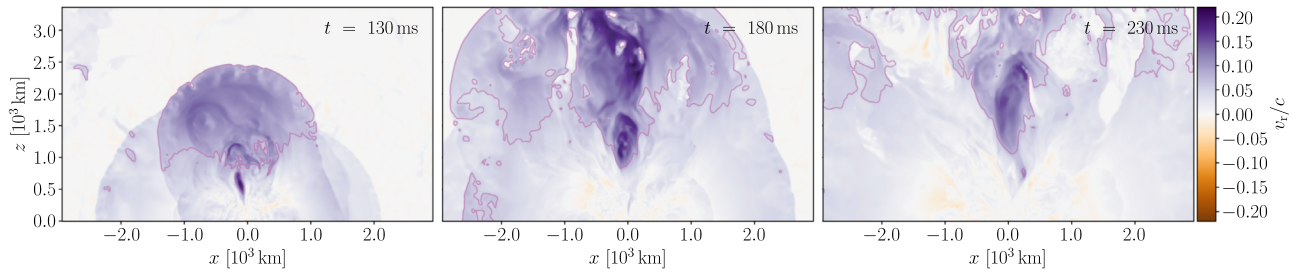


**Figure 1.** Meridional view of radial wind velocities at 130, 180, and 230 ms after merger. The magenta contour lines indicate unbound matter (according to the geodesic criterion  $-u_r > 1$ , see the text).

adopt the conservative geodesic criterion  $-u_r > 1$  (Hotokezaka et al. 2013).

The early contribution of dynamical ejecta can be clearly distinguished from the MNS wind contribution. We find  $\simeq 0.01 M_\odot$  of dynamical ejecta expelled within less than 10 ms after merger (with no distinction of tidal and shock-driven ejecta). Having high enough velocity (ranging up to more than  $0.2c$ ), this component could represent a potential candidate to explain the blue kilonova in AT 2017gfo. However, only a fraction of this material would retain a low enough opacity (e.g., Radice et al. 2016) and given that the mass is already smaller than the expected range (i.e.,  $\simeq 0.015\text{--}0.025 M_\odot$ ), the chances of being the dominant source of the blue kilonova appear rather limited. While our results do not exclude that dynamical ejecta could contribute significantly to the blue and/or the red kilonova components of AT 2017gfo, a more precise assessment is beyond the scope of this work.

Turning the attention to the MNS wind, Figure 2 shows how the (total and unbound) mass flow rate at a given distance grows in time up to a maximum and then starts declining, with a clear suppression toward the end of the simulation ( $\simeq 255$  ms after merger). The final decline is quite regular and can be reproduced very well with an exponential decay. Based on this, we can extrapolate in time to obtain the full evolution. At this point, it is possible to compute the total and unbound cumulative masses in the late-time limit (assuming that no collapse to a BH occurs) for a given set of distances. The result is given in Figure 3. As expected, the total mass decreases with distance, but the unbound fraction increases, converging toward the large distance limit in which the two coincide (i.e., all the outflowing material far away from the MNS is unbound). The ultimate ejecta mass will then be contained within the range of values defined by the total and unbound masses at the largest distance that we probe, 2360 km, leading to  $M_{\text{ej, wind}} \simeq 0.010 - 0.028 M_\odot$ . We note that this refers to the MNS wind only, excluding the dynamical ejecta contribution.

The above mass would be sufficient to explain the blue kilonova in AT 2017gfo. While limited to a single physical model, this result shows that, in terms of mass, magnetically driven MNS winds represent a valid (and promising) possibility.<sup>7</sup>

The possible collapse to a BH would interrupt the mass-ejection process via the MNS wind. When this occurs, only the material within  $\approx 200\text{--}300$  km from the BH is influenced by the collapse, while the rest is almost unaffected (Ciolfi et al. 2019).

<sup>7</sup> Conversely, explaining the full (blue and red) kilonova mass, which is most likely  $\gtrsim 0.05 M_\odot$  (e.g., Kasen et al. 2017; Villar et al. 2017, but see also Kawaguchi et al. 2018), seems challenging. This favors the eventual collapse to a BH and the presence of a massive wind from its accretion disk as an additional necessary contribution (in particular for the red kilonova; e.g., Siegel & Metzger 2018).

Taking our present simulation as a reference, we can then monitor the cumulative mass outflow across the spherical surface of radius 300 km and estimate what fraction of mass would actually be expelled within a given collapse time. We find that 90% of the mass outflow (from 5% to 95%) occurs between 54 and 189 ms after merger, while after 285 ms further outflow accounts for less than 1% of the total. This indicates that a collapse within about 50 ms would almost entirely suppress this ejecta component. On the other hand, any lifetime beyond  $\approx 200$  ms would lead to a similar ejecta mass, as after this time additional contributions become negligible.<sup>8</sup>

As shown in Figure 1, MNS wind radial velocities reach over  $0.2c$ , in particular along polar directions within  $\simeq 15^\circ$  from the the spin axis. Overall, the velocity of the unbound material spans the range  $\simeq 0.1\text{--}0.2c$ . These values are consistent with the lower end of the range inferred from observational data (i.e.,  $\simeq 0.2\text{--}0.3c$ ). We note, however, that various effects not included in our simulation could further enhance these velocities. One effect is nuclear recombination of free nucleons into  $\alpha$ -particles, in which part of the available nuclear binding energy would be ultimately converted into outflowing motion (e.g., Siegel & Metzger 2018). Then, the presence of a relativistic jet launched at later times and drilling through the MNS ejecta (necessary to explain the short gamma-ray burst GRB 170817A; e.g., Abbott et al. 2017c; Mooley et al. 2018; Ghirlanda et al. 2019) would also slightly increase the kinetic energy of the latter (to be quantified via actual jet simulations). Neutrino radiation from the MNS could also lead to a higher radial kinetic energy per baryon within the magnetically driven ejecta (e.g., Perego et al. 2014), even though this remains to be demonstrated in a full magnetized BNS merger simulation including neutrino emission and neutrino heating. In addition to these effects, we also note that in our simulation an artificial floor density of  $\simeq 6.3 \times 10^4 \text{ g cm}^{-3}$  is imposed, which could be slowing down the MNS wind in a non-negligible way (e.g., Martin et al. 2018).

As additional note, the presence of a non-negligible amount of shock-driven dynamical ejecta along the polar direction would imply a reprocessing of the kilonova emission from the MNS wind, which may result in a significant increase of the observed photospheric velocity. This effect, illustrated in Kawaguchi et al. (2018), represents another viable way to further improve the accordance between the blue kilonova observations and the somewhat slower MNS wind obtained here.

The angular distribution of the MNS ejecta extends up to a half-opening angle of more than  $60^\circ$ . The monotonic decrease in

<sup>8</sup> At much later time, if no collapse has occurred, the fallback of material may still lead to additional episodes of mass ejection, but we do not speculate here on whether this is possible and/or quantitatively relevant. Fallback material may also leave an imprint in the properties of a later jet (e.g., Lamb et al. 2020).

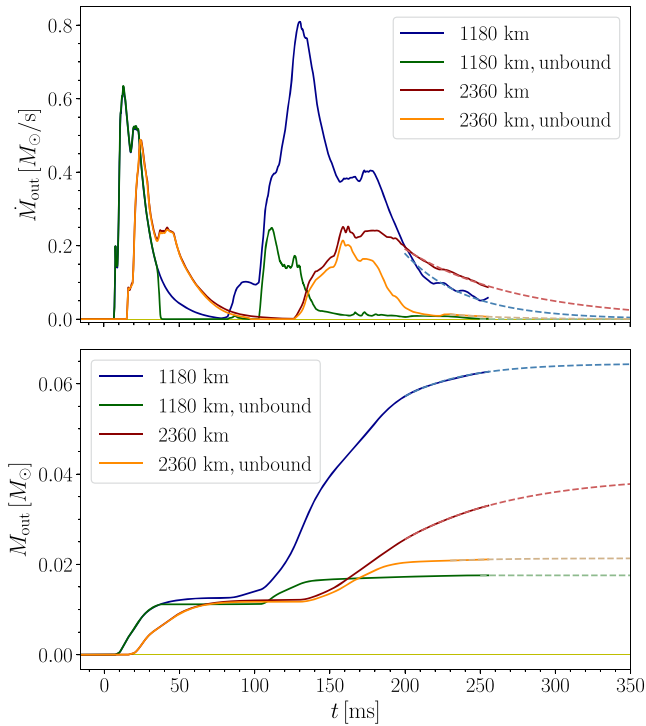


**Figure 2.** Top panel: time evolution of the mass flow rates across spherical surfaces of radius 1180 and 2360 km, for both the total mass and the unbound mass. Dashed lines correspond to the exponential profiles used for the extrapolation at later times. Bottom panel: analogous plot for the cumulative mass flows.

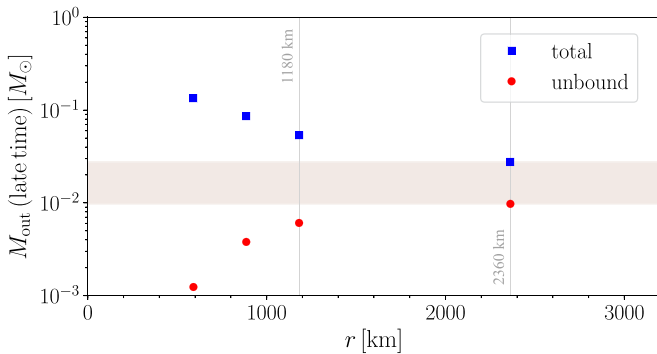


**Figure 3.** Total and unbound cumulative mass flowing across spherical surfaces of different radii in the late time limit (i.e., maximum achievable for a sufficiently long-lived MNS). The values refer to the MNS wind only, excluding dynamical ejecta contributions. The ultimate ejecta mass (in the late time and large distance limit) has to be within the range defined by the shaded region.

velocity from the axis to higher polar angles can be approximately reproduced by  $v_r(\theta) = v_r(\theta = 0) / [1 + (\theta/\theta_0)^a]$ , where the parameters  $(\theta_0, a)$  vary significantly in time. For instance, at 120 ms after merger  $\theta_0 \simeq 43^\circ.5$ ,  $a \simeq 3.46$  (error < 15%), while at 180 ms after merger  $\theta_0 \simeq 25^\circ.8$ ,  $a \simeq 1.14$  (error < 7%).

We close the present Section with a note on the opacity. As confirmed in a number of studies (e.g., Perego et al. 2014; Fujibayashi et al. 2018), neutrino irradiation (not included here) has the effect of significantly raising the electron fraction of the MNS wind material, leading to ejecta having  $Y_e \simeq 0.25\text{--}0.40$ . The  $r$ -process nucleosynthesis is then mostly limited to heavy elements with  $A \lesssim 140$  and the resulting opacity remains rather

low, i.e.,  $\sim 0.1\text{--}1 \text{ cm}^2 \text{ g}^{-1}$  (e.g., Tanaka et al. 2018). This is in agreement with the blue kilonova requirement.

#### 4. Conclusions

We analyzed the outcome of a BNS merger simulation showing the formation of a magnetically driven collimated outflow along the rotation axis of the MNS remnant. Such an outflow is associated with the gradual build-up of a helical magnetic field structure due to the action of the strong differential rotation within the MNS core. We found that the magnetically enhanced mass flow rate and velocity in the polar direction leads to an ejecta component that would represent a viable explanation for the puzzling blue kilonova in AT 2017gfo.<sup>9</sup> In particular, for the case at hand, we obtained a robust estimate for the mass of the unbound material in the range  $\simeq 0.010\text{--}0.028 M_\odot$ , with 95% of the mass ejection occurring within  $\simeq 190$  ms after merger. This result shows that MNS baryon winds, when a magnetically driven collimated outflow is able to emerge, can lead to an ejecta mass that is consistent with the blue kilonova observation of 2017 August. The radial velocities that we found are limited to a maximum of  $\simeq 0.2c$ , consistent with the lower end of the range estimated from the observations. We also discuss possible effects that, when taken into account, could further increase the ejecta velocities. Finally, we noted that the expected opacities of the MNS wind material are also fully compatible with a blue kilonova.

Our findings, in combination with those reported in Ciolfi (2020a), support a scenario for the BNS merger of 2017 August in which (i) the blue kilonova was mainly powered by radioactive decay within the magnetically driven baryon wind from a metastable MNS, possibly with a significant contribution from shock-driven dynamical ejecta, (ii) the eventual collapse of the MNS formed an accreting BH system able to launch the relativistic jet that powered the short gamma-ray burst GRB 170817A (e.g., Abbott et al. 2017c; Mooley et al. 2018; Ghirlanda et al. 2019), and (iii) the baryon wind from the accretion disk around the BH provided the dominant contribution to the red kilonova.

While we refer here to a single merger simulation, a more exhaustive understanding of magnetically driven MNS winds will require the exploration of a large variety of BNS systems and their diverse physical conditions (including different EOS; e.g., Ai et al. 2020). Nonetheless, the present study already provides new important indications on the qualitative properties of this mass-ejection channel. For the first time, we traced the full process, from the initial development of the baryon wind until the suppression of the outgoing mass flow. We found that the wind material is almost entirely expelled within a limited time window, which for the specific case is between about 50 and 200 ms after merger. On the one hand, this implies a lower limit on the MNS lifetime when this ejecta component is present (here  $\gtrsim 50$  ms). On the other hand, it shows that there is a maximum achievable ejecta mass via this channel that remains nearly unchanged for any MNS lifetime above a certain value (here  $\approx 200$  ms). The time at which mass ejection is mostly over also marks the beginning of the separation between the unbound material moving outwards and

<sup>9</sup> We note that the same ejection mechanism may also offer a viable explanation for other blue kilonova candidates found in association with earlier short GRBs (e.g., Troja et al. 2018; Lamb et al. 2019).

the bound material that is starting to fall back toward the central object. Furthermore, we found that the ejecta radial velocity is maximum along the MNS spin axis and smoothly decreases for increasing polar angles, up to the full angular extension of more than  $60^\circ$ .

Overall, our results confirm the crucial role played by magnetic fields in the post-merger evolution, and in particular in the ejection of mass during the MNS phase (see also Ciolfi 2020b). We encourage further investigation on magnetically driven MNS winds via full magnetized BNS merger simulations, possibly including, as a first necessary improvement, neutrino radiation along with finite temperature and composition dependent EOS.

We thank Brian D. Metzger, Wolfgang Kastaun, Albino Perego, and Daniel M. Siegel for useful comments. J.V.K. kindly acknowledges the CARIPARO Foundation for funding his PhD fellowship within the PhD School in Physics at the University of Padova. Numerical simulations were performed on the cluster MARCONI at CINECA (Bologna, Italy). We acknowledge a CINECA award under the MoU INAF-CINECA initiative (allocation INA17\_C3A23), for the availability of high performance computing resources and support. In addition, part of the numerical calculations have been made possible through a CINECA-INFN agreement, providing access to further resources (allocation INF19\_teongrav).

### ORCID iDs

Riccardo Ciolfi  <https://orcid.org/0000-0003-3140-8933>

Jay Vijay Kalinani  <https://orcid.org/0000-0002-2945-1142>

### References

- Abbott, B. P., Abbott, R., Abbott, T. D., et al. 2017a, *PhRvL*, **119**, 161101  
 Abbott, B. P., Abbott, R., Abbott, T. D., et al. 2017b, *ApJL*, **848**, L12  
 Abbott, B. P., Abbott, R., Abbott, T. D., et al. 2017c, *ApJL*, **848**, L13  
 Abbott, B. P., Abbott, R., Abbott, T. D., et al. 2019, *PhRvX*, **9**, 011001  
 Ai, S., Gao, H., & Zhang, B. 2020, *ApJ*, **893**, 146  
 Akmal, A., Pandharipande, V. R., & Ravenhall, D. G. 1998, *PhRvC*, **58**, 1804  
 Balbus, S. A., & Hawley, J. F. 1991, *ApJ*, **376**, 214  
 Bauswein, A., Goriely, S., & Janka, H. T. 2013, *ApJ*, **773**, 78  
 Ciolfi, R. 2020a, *MNRAS Lett.*, **495**, L66  
 Ciolfi, R. 2020b, *GRGr*, **52**, 59  
 Ciolfi, R., Kastaun, W., Kalinani, J. V., & Giacomazzo, B. 2019, *PhRvD*, **100**, 023005  
 Cowperthwaite, P. S., Berger, E., Villar, V. A., et al. 2017, *ApJL*, **848**, L17  
 Endrizzi, A., Ciolfi, R., Giacomazzo, B., Kastaun, W., & Kawamura, T. 2016, *CQGra*, **33**, 164001  
 Fujibayashi, S., Kiuchi, K., Nishimura, N., Sekiguchi, Y., & Shibata, M. 2018, *ApJ*, **860**, 64  
 Ghirlanda, G., Salafia, O. S., Paragi, Z., et al. 2019, *Sci*, **363**, 968  
 Hotokezaka, K., Kiuchi, K., Kyutoku, K., et al. 2013, *PhRvD*, **88**, 044026  
 Kasen, D., Metzger, B., Barnes, J., Quataert, E., & Ramirez-Ruiz, E. 2017, *Natur*, **551**, 80  
 Kawaguchi, K., Shibata, M., & Tanaka, M. 2018, *ApJL*, **865**, L21  
 Kiuchi, K., Cerdá-Durán, P., Kyutoku, K., Sekiguchi, Y., & Shibata, M. 2015, *PhRvD*, **92**, 124034  
 Kiuchi, K., Kyutoku, K., Sekiguchi, Y., & Shibata, M. 2018, *PhRvD*, **97**, 124039  
 Kiuchi, K., Kyutoku, K., & Shibata, M. 2012, *PhRvD*, **86**, 064008  
 Lamb, G. P., Levan, A. J., & Tanvir, N. R. 2020, *ApJ*, **899**, 105  
 Lamb, G. P., Tanvir, N. R., Levan, A. J., et al. 2019, *ApJ*, **883**, 48  
 Lattimer, J. M., & Schramm, D. N. 1974, *ApJL*, **192**, L145  
 Li, L.-X., & Paczyński, B. 1998, *ApJL*, **507**, L59  
 Martin, D., Perego, A., Kastaun, W., & Arcones, A. 2018, *CQGra*, **35**, 034001  
 Metzger, B. D. 2019, *LRR*, **23**, 1  
 Metzger, B. D., Martínez-Pinedo, G., Darbha, S., et al. 2010, *MNRAS*, **406**, 2650  
 Metzger, B. D., Thompson, T. A., & Quataert, E. 2018, *ApJL*, **856**, 101  
 Mooley, K. P., Deller, A. T., Gottlieb, O., et al. 2018, *Natur*, **561**, 355  
 Mösta, P., Radice, D., Haas, R., Schnetter, E., & Bernuzzi, S. 2020, *arXiv:2003.06043*  
 Nedora, V., Bernuzzi, S., Radice, D., et al. 2019, *ApJL*, **886**, L30  
 Perego, A., Radice, D., & Bernuzzi, S. 2017, *ApJL*, **850**, L37  
 Perego, A., Rosswog, S., Cabezón, R. M., et al. 2014, *MNRAS*, **443**, 3134  
 Pian, E., D'Avanzo, P., Benetti, S., et al. 2017, *Natur*, **551**, 67  
 Radice, D., Galeazzi, F., Lippuner, J., et al. 2016, *MNRAS*, **460**, 3255  
 Ruiz, M., Lang, R. N., Paschalidis, V., & Shapiro, S. L. 2016, *ApJL*, **824**, L6  
 Ruiz, M., Shapiro, S. L., & Tsokaros, A. 2018, *PhRvD*, **97**, 021501  
 Shibata, M., Suwa, Y., Kiuchi, K., & Ioka, K. 2011, *ApJL*, **734**, L36  
 Siegel, D. M. 2019, *EPJA*, **55**, 203  
 Siegel, D. M., Ciolfi, R., Harte, A. I., & Rezzolla, L. 2013, *PhRvD*, **87**, 121302  
 Siegel, D. M., Ciolfi, R., & Rezzolla, L. 2014, *ApJL*, **785**, L6  
 Siegel, D. M., & Metzger, B. D. 2018, *ApJ*, **858**, 52  
 Symbalisty, E., & Schramm, D. N. 1982, *ApL*, **22**, 143  
 Tanaka, M., Kato, D., Gaigalas, G., et al. 2018, *ApJ*, **852**, 109  
 Troja, E., Ryan, G., Piro, L., et al. 2018, *NatCo*, **9**, 4089  
 Villar, V. A., Guillochon, J., Berger, E., et al. 2017, *ApJL*, **851**, L21